Polymer Chemistry

ROYAL SOCIETY OF CHEMISTRY

PAPER

View Article Online
View Journal | View Issue

Cite this: *Polym. Chem.*, 2024, **15**, 2642

Synthesis of carbazole–chalcone bis-oxime esters (CCBOEs) as blue light photoinitiators of polymerization†

Zheng Liu,‡[a] Yijun Zhang, ‡[b] Ji Feng,[b] Bin Song,[b] Tong Gao,[b] Céline Dietlin,[b] Fabrice Morlet-Savary,[b] Michael Schmitt, [b] Didier Gigmes, [a] Frédéric Dumur *[a] and Jacques Lalevée *[b]

Received 23rd April 2024,
Accepted 4th June 2024

DOI: 10.1039/d4py00454j

rsc.li/polymers

In this work, a series of sixteen asymmetrically substituted bis-oxime esters, CCBOEs, bearing different substituents on the oxime ester sides were designed as Type I photoinitiators for photopolymerization experiments done with blue light (405, 450 and 470 nm) under low light intensities (use of LEDs as the light sources). These natural product-inspired compounds showed a strong absorption in the visible range and exhibited a fast cleavage of the oxime ester groups upon photoexcitation, enabling complete oxime ester consumption to be achieved within 2 s. By using the above-mentioned light sources, three CCBOEs (namely CCBOE1, CCBOE4, and CCBOE5) bearing alkyl substituents on the oxime ester sides exhibited high acrylate monomer conversions but also good thermal polymerization abilities, evidencing their dual activation modes. By means of electron spin resonance (ESR) experiments, the formation of free radicals was demonstrated and led to the proposal of a plausible initiation mechanism. The hypothesis of homolytic cleavage of the N–O bond was also supported by the detection of the CO_2 absorption peak by Fourier Transform Infrared spectroscopy (FT-IR). The initiating mechanism was also investigated by theoretical calculations, enabling the excited state involved in the cleavage process to be determined. Finally, high-resolution 3D patterns were successfully fabricated using the CCBOE5/TMPTA system through direct laser writing (DLW).

A Introduction

Visible light photopolymerization constitutes a green approach for generating free radicals.[1–3] This technology finds extensive applications in diverse fields such as coatings, adhesives, graphic materials, dental materials, and 3D printing technology due to its ease of handling, robustness, efficiency and low energy consumption.[4–11] Oxime esters (OXEs), categorized as Type I photoinitiators, can generate upon photoexcitation free radicals by means of a homolytic cleavage of the N–O bond and a decarboxylation reaction, making these structures the focus of numerous studies in the last three years.[12–14]

In addition to the advantages of being easily synthesizable, at low cost and with high reaction yields, the oxime ester groups can be connected to a wide range of chromophores such as carbazole, phenothiazine, anthracene, pyrene, coumarin, and chalcone so that the absorption spectra of oxime esters can be facilely adjusted.[15–17] Chalcones are biosourced but also bioinspired α,β-unsaturated ketones that strongly absorb in the visible range due to the excellent electronic delocalization existing within these structures. Because of their extended π-conjugated structures, chalcones are also excellent electron donating groups,[18,19] and chalcones have been extensively used as electron donors for various two and three-component photoinitiating systems.[20–22] Technically, chalcones belong to the flavonoid family and these structures can be commonly found in plants. Chalcones are notably responsible for the color of numerous flowers and fruits.[23–25] Chalcones are also studied for their biological activities and numerous natural chalcones exhibit pharmacological and biological properties.[26–28] From the synthetic viewpoint, chalcones can be easily synthesized by means of a Claisen–Schmidt condensation under basic conditions, starting from cheap and easily available reagents.[29–31] Benefiting from this easiness of synthesis, numerous chalcones that cannot be found in Nature have been prepared over the years, with a major contribution in drug development. Parallel to their biological activities, chalcones have emerged as prominent scaffolds for the design

[a]*Aix Marseille Univ, CNRS, ICR UMR 7273, F-13397 Marseille, France. E-mail: frederic.dumur@univ-amu.fr*
[b]*Université de Haute-Alsace, CNRS, IS2M UMR 7361, F-68100 Mulhouse, France. E-mail: jacques.lalevee@uha.fr*

†Electronic supplementary information (ESI) available. See DOI: https://doi.org/10.1039/d4py00454j

‡These authors equally contributed to this work.

of Type II photoinitiators. In this field, major advances in the design of chalcone-based photoinitiators have been brought by the research groups of Jacques Lalevée, Jun Nie, Jingqing Qu and Tao Wang.[22,32–35] So far, only two works about chalcone-based OXEs have been reported in the literature. In 2022, Wu *et al.* designed and synthesized a series of three D–π-A–π-A′ bis-chalcone-based OXEs, namely TA1, TA2 and TA3.[36] The final conversion obtained during the free radical polymerization (FRP) of 1,6-hexanediol diacrylate (HDDA) as the monomer reached a maximum of 66% after irradiation for 30 min with a 405 nm light source. Furthermore, the photopolymerization efficiencies of TA2 under irradiation at 455, 470, and 490 nm with LEDs were remarkable, with final monomer conversions of 75, 79 and 72%, respectively. However, their polymerization abilities have not been examined for the FRP of trimethylolpropane triacrylate (TMPTA). In 2023, Zhang *et al.* examined the polymerization efficiencies of a series of pyrene–chalcone OXEs in TMPTA.[37] Unfortunately, the highest final conversion was only 47% after irradiation with a 405 nm LED for 200 s. This under-performance was assigned to the presence of a benzene ring introduced between the oxime ester groups and the pyrene–chalcone chromophore. With this group acting as an electronic insulator, the efficiency of the energy transfer from the chromophore towards the photocleavable group was drastically reduced, adversely affecting the photoinitiating ability.

So far, there has been only one report mentioning the utilization of bis-oxime esters for visible light photopolymerization. In 2022, Zhang and coworkers ingeniously devised two distinct phenothiazine-based bis-OXEs and employed these two structures for the polymerization of TMPTA.[38] After 800 s of exposure to a 405 nm LED, the polymerization efficiency was impressive. OXE-A1 and OXE-B2 achieved final acrylate function conversions of 80% and 74%, respectively. Hence, it was concluded that by enhancing the number of oxime ester functionalities per molecule, more radicals can be produced, improving the reactivity of these structures. In light of these results, we considered the introduction of two OXE functionalities per molecule as an efficient strategy to enhance the photopolymerization efficiency of our chalcone-based photoinitiators.

Given that blue light falls within the visible spectrum, it presents the advantages of controllability of the emission range and energy consumption when LEDs are used as the light sources, and a better light penetration can be obtained compared to UV light.[39,40] Opting for OXEs for the FRP of TMPTA under blue light holds merit, especially when compared to the commercially available diphenyl(2,4,6-trimethylbenzoyl)phosphine oxide (TPO) which lacks absorption at 455 nm.[15] However, to date, there is currently only one report concerning the FRP of TMPTA using OXEs under blue light. The final conversion obtained with the *N*-naphthalimide ester derivative NPIE1, as prepared by Liu *et al.*, reached only 44% after 200 s of exposure to 455 nm radiation.[41]

Given the ease of modification of the 6-position of carbazole, this project initially conceptualized to synthesize a series of bis-oxime esters with the chalcone group introduced at the 6-position of carbazole. The chemical structures of these CCBOEs have been confirmed by means of ^{1}H and ^{13}C NMR, and mass spectrometry (MS) analyses. Their photophysical and photolysis properties were characterized using UV-visible absorption spectroscopy. FT-IR served the dual purpose of not only evaluating the polymerization efficacy of the CCBOEs during the FRP of TMPTA at 405 nm, but also with blue light (450 and 470 nm), and to record the changes in CO_2 content during photopolymerization. The differences in the cleavage efficiencies of the CCBOEs in TMPTA were elucidated through a comparison of the singlet excited state energies and the triplet excited state energies with the N–O bond dissociation energies, along with the fluorescence lifetimes. Differential Scanning Calorimetry (DSC) was employed to investigate the thermal polymerization behaviors of the different CCBOEs in TMPTA. The chemical mechanism of CCBOEs was comprehensively investigated using FT-IR, ESR, UV-visible absorption and fluorescence spectroscopy, along with theoretical calculations. The selected CCBOE5 was used to print predefined 3D patterns using direct laser writing (DLW), and the resolution of the resulting structures was observed through numerical optical microscopy.

B Results and discussion

B.1 Synthesis of the dyes

The synthesis of the CCBOEs involved five steps, starting from 9-ethyl-9*H*-carbazole **C1** (see Scheme 1 and the general information in the ESI†). Firstly, 9-ethylcarbazole **C1** underwent a Vilsmeier–Haack reaction with $POCl_3$ and DMF, producing 9-ethyl-9*H*-carbazole-3-carbaldehyde **C2** in 92.4% yield. Subsequently, the product **C2** underwent a Claisen–Schmidt condensation with 1,4-diacetylbenzene in methanol using 40% KOH as the base, yielding the carbazole-based chalcone **C3** as a *trans* isomer (89.2% yield). Considering that the reaction was performed at room temperature, formation of the thermodynamic product (the *trans* form) was favored over the kinetic one (the *cis* form). In a third step, recognizing the high reactivity at the 6th position of the carbazole, an acetyl group could be selectively introduced at this position by an acylation reaction, furnishing **C4** in 95.7% yield. With this precursor prepared, **C4** was converted to the bis-oxime CCBOE0 using inexpensive reagents such as hydroxylamine hydrochloride and sodium acetate in a ternary mixture of solvents (methanol, water and THF), providing CCBOE0 in 97.6% yield. Finally, utilizing triethylamine as the base, the oxime CCBOE0 was esterified using the appropriate acid chlorides so that sixteen bifunctional OXEs CCBOE1–CCBOE16 could be produced with different substituents (alkyl and aryl groups).

B.2 Light absorption of properties

The UV-visible absorption spectra of these CCBOEs in dichloromethane (DCM) are shown in Fig. 1, and their maximum absorption wavelengths (λ_{max}) and molar extinction coefficients (ε) at λ_{max}, 405, 450 and 470 nm are listed in Table 1, respectively. Apart from CCBOE0, all of the com-

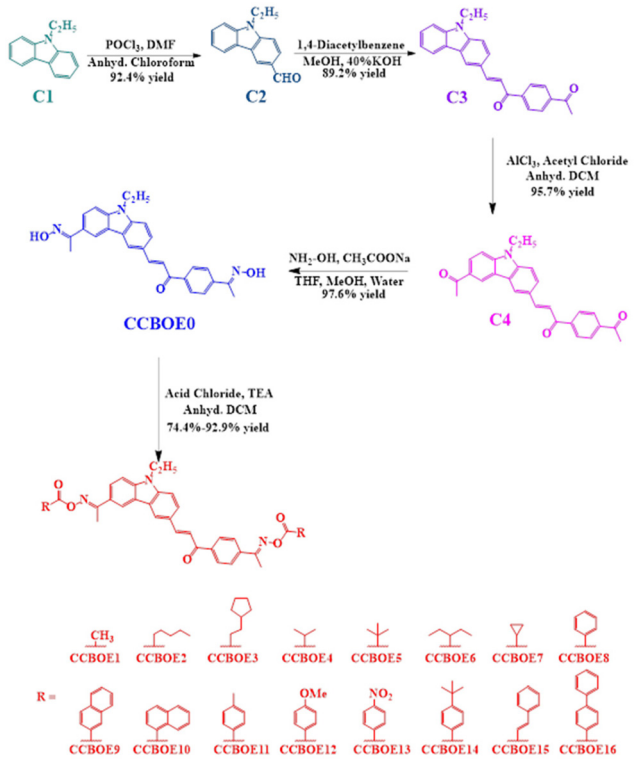

Scheme 1 Synthetic routes to CCBOEs.

pounds exhibited an excellent solubility in DCM. As shown in Fig. 1, the CCBOEs displayed a broad absorption band extending up to 500 nm, and their λ_{max} are located around 389 to 392 nm (see Table 1). As shown in Table 1, the different substituents don't cause any obvious blueshift or redshift of the λ_{max}, but they affect the molar extinction coefficients $\varepsilon_{405\ nm}$, $\varepsilon_{450\ nm}$ and $\varepsilon_{470\ nm}$. This can be attributed to the fact that the different substituents on the oxime ester sides are not in conjugation with the rest of the molecule, so their influence is restricted to the molar extinction coefficients and not to the positions of the absorption spectra.

All of the CCBOEs exhibited high molar extinction coefficients at 405 nm. CCBOE15 and CCBOE8 showed the highest and the lowest molar extinction coefficients, with ε values of 16 100 M^{-1} cm^{-1} and 6700 M^{-1} cm^{-1}, respectively. It's noteworthy that all of

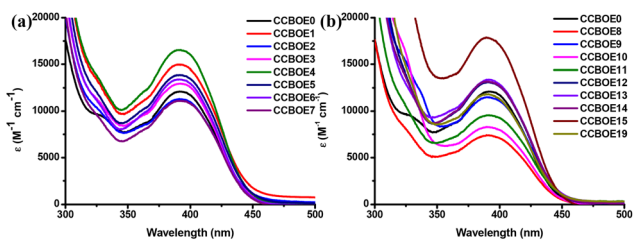

Fig. 1 UV-visible absorption spectra of CCBOEs (concentration: 2 × 10^{-5} M) in DCM.

Table 1 Light absorption properties of CCBOEs

CCBOEs	λ_{max} (nm)	ε_{max} (M^{-1} cm^{-1})	$\varepsilon_{405\ nm}$ (M^{-1} cm^{-1})	$\varepsilon_{450\ nm}$ (M^{-1} cm^{-1})	$\varepsilon_{470\ nm}$ (M^{-1} cm^{-1})
CCBOE0	391	12 100	11 000	800	100
CCBOE1	390	15 000	13 700	1800	900
CCBOE2	391	11 300	10 300	1200	400
CCBOE3	392	13 000	11 800	900	100
CCBOE4	392	16 600	15 200	1100	0
CCBOE5	391	13 900	12 800	1200	100
CCBOE6	391	13 400	12 200	800	200
CCBOE7	392	11 100	10 300	600	0
CCBOE8	389	7400	6700	500	0
CCBOE9	391	11 500	10 500	1100	400
CCBOE10	389	8300	7500	600	0
CCBOE11	392	9600	8800	1000	400
CCBOE12	391	13 100	12 000	900	200
CCBOE13	391	13 400	12 200	1200	400
CCBOE14	389	13 200	12 000	1100	200
CCBOE15	389	17 900	16 100	900	0
CCBOE16	391	11 800	10 600	1100	400

the CCBOEs display significant absorptions at longer wavelengths (450 and 470 nm), indicative of their potential to serve as initiators for the polymerization of acrylate monomers under 450 nm and 470 nm LEDs. In conclusion, the bis-oxime esters, CCBOEs, featuring carbazole and chalcone groups exhibited significant absorptions in the visible range, making these structures excellent candidates for photopolymerization experiments done at 405, 450 and 470 nm.

B.3 Steady-state photolysis

In order to explore the photocleavage properties of CCBOEs, steady-state photolysis experiments were conducted at 405 nm and at 450 nm with LEDs for different irradiation times (see Fig. S1 and S2†). Fig. 2 summarizes the dye consumptions determined for the different CCBOEs.

Interestingly, except for CCBOE0 which is not an oxime ester but just an oxime, alkyl-substituted and aryl-substituted CCBOEs showed similar photodegradation patterns, wherein the absorption intensity at the λ_{max} rapidly decreased within 1 s of exposure to 405 nm LED illumination. After this first fast decrease step, the λ_{max} of all of the CCBOEs remained almost unchanged after 15 s of irradiation. In fact, the decomposition of the oxime esters is a competitive reaction channel to the *cis*/*trans* isomerization, adversely affecting the cleavage process. This point was evidenced by CCBOE0. In the absence of the oxime ester group, CCBOE0 exhibited a similar photolysis process, attributed solely to the *trans*–*cis* isomerization of the carbazole–chalcone structure upon irradiation with a 405 nm LED.[42–44]

Noticeably, a decrease of the photolysis efficiency was also demonstrated upon irradiation at 450 nm. Even after 15 s of irradiation, the absorption intensity still decreased, evidencing that the photocleavage had not ended. After 120 s of irradiation with a 450 nm LED, the decrease of the absorption intensities at the λ_{max} for all CCBOEs was far lower compared to that determined at 405 nm. In comparison to the 22% dye

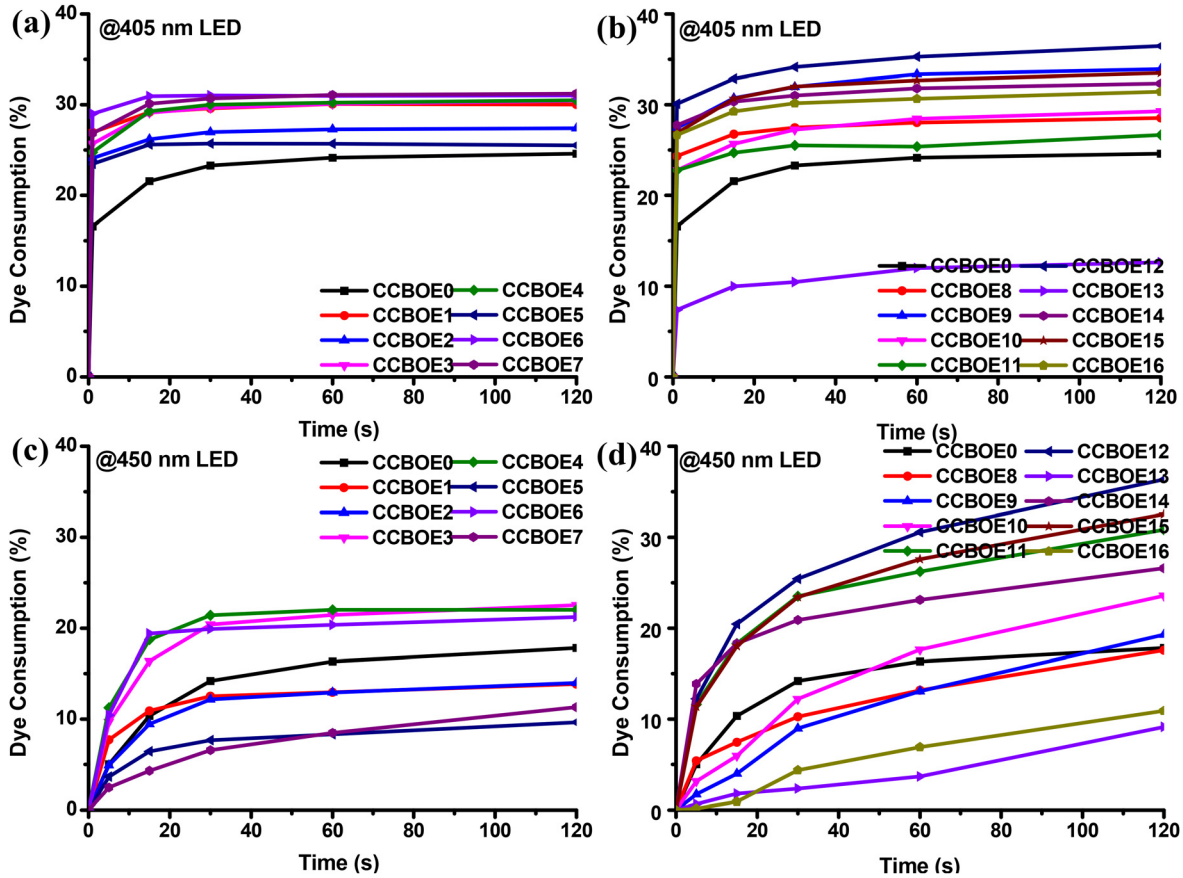

Fig. 2 Dye consumptions of CCBOEs (concentration: 2×10^{-5} M) in DCM upon irradiation with a 405 nm LED (a and b) and a 450 nm LED (c and d).

consumption for CCBOE0, all of the CCBOEs except CCBOE13 exhibited dye consumption higher than 25% after 1 s of irradiation with a 405 nm LED. Even with an increased irradiation time with the 405 nm LED, after 120 s, the rate of decrease in absorption values at the λ_{max} for the CCBOEs remained significantly higher than that of CCBOE0. Conversely, the dye consumption of the CCBOEs after 450 nm LED irradiation markedly decreased. Even after 120 s, the final dye consumption for all of the alkyl-substituted CCBOEs, CCBOE1–CCBOE7, did not exceed 23%. Encouragingly, some aryl-substituted CCBOEs exhibited higher dye consumptions than CCBOE0. This indicates that the CCBOEs are less reactive at 450 nm than 405 nm and this is directly related to a decrease of the molar extinction coefficients. Overall, the photolysis experiments clearly evidenced the competition existing between photocleavage of the oxime ester groups and the *trans–cis* isomerization of the chalcone core. At longer wavelengths, the two competitive processes are slower, photons at 450 nm being less energetic than the 405 nm ones.

Consequently, bis-oxime esters based on the carbazole–chalcone scaffold exhibited a fast photodegradation phenomenon upon visible light exposure. CCBOEs are thus good candidates for initiating the polymerization of acrylate monomers at 405 nm but also at longer wavelengths.

B.4 Free radical photopolymerization

Fig. 3 presents the photopolymerization curves of CCBOEs in thin samples under 405 nm, 450 nm and 470 nm LED sources, respectively, while Table 2 provides the final conversions (FCs) obtained for the different CCBOEs. Except for CCBOE0, CCBOE13 and CCBOE16, all the other CCBOEs displayed an excellent solubility in TMPTA. What is exciting is that in thin samples and upon irradiation with an LED at 405 nm, the FCs obtained for the trifunctional monomer TMPTA using CCBOE1, CCBOE3, CCBOE4 and CCBOE5 possessing alkyl groups on the oxime ester sides were high, exceeding 70%. Interestingly, the highest FC was obtained with CCBOE5, peaking at 77% after irradiation for 300 s (see Fig. 3a and b). Conversely, none of the CCBOEs possessing aromatic rings on the oxime ester side could furnish high monomer conversions and all FCs were lower than 70%. This can be attributed to the fact that, while aromatic-substituted CCBOEs can generate aryl radicals when exposed to a 405 nm LED, their reactivities are considerably reduced compared to those of alkyl radicals due to an electronic stabilization. As a result of this, alkyl radicals demonstrate an elevated reactivity in photopolymerization reactions. Meanwhile, as shown in Fig. 3c and d, due to the varying absorptions of the different CCBOEs at 450 nm, the

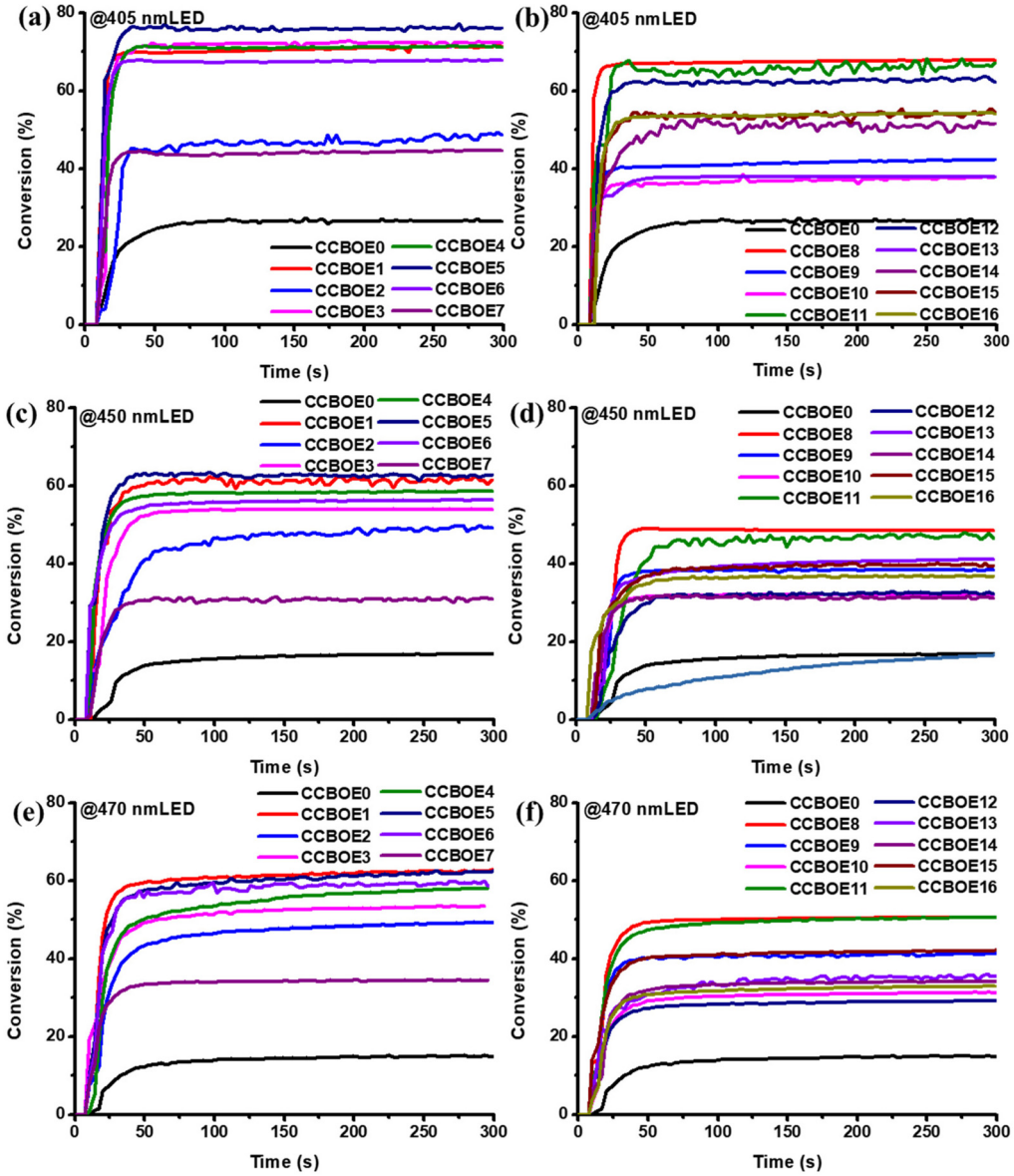

Fig. 3 Photopolymerization profiles of TMPTA in a laminate (25 μm) upon exposure to a 405 nm LED (a and b), a 450 nm LED (c and d) and a 470 nm LED (e and f), in the presence of different CCBOEs (2×10^{-5} mol g^{-1} in TMPTA). The irradiation starts at t = 10 s.

efficiency of the N–O bond cleavage differs significantly, resulting in major differences in the photopolymerization kinetics of TMPTA. Compared to the absorption at 405 nm, the absorption values of CCBOEs at 450 nm are significantly reduced, with an absorption maximum of only 1200 M^{-1} cm^{-1}. Fortunately, CCBOEs containing alkyl and aryl groups demonstrate a detectable activity in initiating the FRP of TMPTA under 450 nm light irradiation. In comparison to CCBOE0 and aryl-substituted CCBOEs, CCBOE1 and CCBOE5 achieved FCs of 63%. This indicates that these CCBOEs are also sensitive to blue light, effectively triggering and promoting photopolymerization reactions under a 450 nm LED.

Subsequently, in order to determine until which wavelength a polymerization could be still induced with the CCBOEs, a longer irradiation wavelength *i.e.* an LED emitting at 470 nm was employed for the corresponding tests (see Fig. 3e and f). Excitingly, even at 470 nm where the CCBOEs exhibit lower absorption properties, the final conversions after 300 s of irradiation with a 470 nm LED are comparable to those under a 450 nm LED light source. Both CCBOE1 and CCBOE5 achieved an FC of 63%, while CCBOE6 attained an FC of 60%.

B.5 The decarboxylation reaction

The singlet excited state energies of the CCBOEs were obtained by normalizing the intersection point of the UV-visible absorption curve and the fluorescence emission curve at the same concentration (2×10^{-5} M) (see Fig. S3 and S4†). The triplet state energies and the bond dissociation energies of the N–O

Table 2 Final acrylate function conversions (FCs) in TMPTA containing different CCBOEs

CCBOEs	25 μm @405 nm LED FCs, %	25 μm @450 nm LED FCs, %	25 μm @470 nm LED FCs, %
CCBOE0	27	17	15
CCBOE1	72	63	63
CCBOE2	64	50	49
CCBOE3	73	54	53
CCBOE4	72	59	58
CCBOE5	77	63	63
CCBOE6	68	56	60
CCBOE7	45	32	35
CCBOE8	68	49	51
CCBOE9	42	39	41
CCBOE10	39	32	31
CCBOE11	68	48	51
CCBOE12	65	33	29
CCBOE13	38	32	36
CCBOE14	57	41	34
CCBOE15	55	40	42
CCBOE16	55	37	33

bond of the CCBOEs were determined by theoretical calculations. Fluorescence lifetimes obtained by time-correlated single-photon counting (TCSPC) are listed in Table S1.† The more negative $\Delta H_{\text{Cleavage S1}}$ and $\Delta H_{\text{Cleavage T1}}$ are, the higher the likelihood of the N–O bond cleavage is.

As shown in Table S1,† CCBOE0, lacking the oxime ester group, exhibits the largest $\Delta H_{\text{Cleavage S1}}$ and $\Delta H_{\text{Cleavage T1}}$. This is unfavorable for the cleavage of the N–O bonds it contains under LED irradiation. However, CCBOE1–CCBOE16 showed lower $\Delta H_{\text{Cleavage S1}}$ values, which are all <0. Interestingly, the $\Delta H_{\text{Cleavage S1}}$ values of the oxime ester groups directly linked to the carbazole group are consistently lower than those determined for the oxime ester groups connected to the benzene ring. These differences of N–O bond energies can be attributed to the distance between the light-absorbing chromophore in the carbazole-based chalcone and the photocleavable groups. Indeed, the energy transfer from the carbazole group to the adjacent oxime ester group is facilitated compared to energy transfer to the oxime ester group standing on the opposite side. Notably, the other oxime ester group is separated from the chromophore by a benzene ring, which acts as a spacer rendering the energy transfer less efficient. A similar phenomenon is observed in $\Delta H_{\text{Cleavage T1}}$, which is higher than $\Delta H_{\text{Cleavage S1}}$. Overall, the negative values of $\Delta H_{\text{Cleavage S1}}$ and $\Delta H_{\text{Cleavage T1}}$ for the CCBOEs indicate the possibility of radical generation from the singlet and the triplet excited states. Besides, the more negative values determined for $\Delta H_{\text{Cleavage S1}}$ is in favor of a photocleavage occurring from the singlet excited state.

Simultaneously, all of the CCBOEs exhibited short fluorescence lifetimes. Even with deconvolution, the experimentally and accurately determined shortest lifetimes are lower than 1.40 ns. This observation confirms that CCBOEs with extremely short excited-state lifetimes are more prone to N–O bond cleavage.

The primary rationale underlying the exceptional initiation efficiency of the CCBOEs in the case of TMPTA is their capacity to generate free radicals through homolytic cleavage of the N–O bond upon exposure to either 405, 450 or 470 nm illumination. At the same time, this process leads to the generation of CO_2, subsequent to the homolytic cleavage, which can be detected by FT-IR. As depicted in Fig. S5, S6 and S7,† appearance of a CO_2 peak at 2337 cm^{-1} could be observed in the infrared spectra of CCBOE1 and CCBOE5 compared to CCBOE0, which remains unaltered following light irradiation for 30, 60 and 90 s. Notably, under 405, 450 and 470 nm LEDs, the characteristic peak of CO_2 was detected for CCBOE1 and CCBOE5 but not for CCBOE0. This highlights the exceptionally high decomposition efficiency of CCBOE1–CCBOE16 after illumination, further substantiating their outstanding polymerization efficiencies in thin samples.

B.6 Proposed chemical mechanism

Based on the above results and reports from the literature, the proposed photochemical mechanism of CCBOEs is depicted in Scheme 2.[17,45,46] CCBOE1–16 is first promoted to the excited state after irradiation with a light source. Irrespective of the excited state pathway (singlet or triplet excited state), a homolytic cleavage of the N–O bond can occur, producing a diiminyl radical located on the carbazole–chalcone structure and two acyloxy/aryloxy radicals. These latter can decarboxylate, producing more reactive radicals, namely alkyl/aryl radicals that can initiate the polymerization of acrylate monomers more readily. This conjecture can be confirmed by electron spin resonance spin trapping (ESR-ST). As shown in Fig. 4, after 15 s of irradiation with a 405 nm LED in *tert*-butylbenzene as the solvent, and by using PBN to capture the free radicals of CCBOE4 and CCBOE5 generated after fragmentation and decarboxylation, the structures of the radicals formed could be identified. The calculated hyperfine coupling constants α_H and α_N are 1.8 G and 14.0 G, respectively, which proves the existence of isopropyl radicals. With α_H and α_N values of 14.5 G and 2.7 G, respectively, the assignment belongs to the *tert*-butyl group.

The efficient cleavage process of acyl-oxy radicals plays a crucial role in promoting the generation of methyl, isopropyl, and *tert*-butyl radicals. Consequently, CCBOE1, CCBOE4, and CCBOE5 exhibited the best performance in photopolymerization among all of the compounds. This observation is consistent with the intense absorption peaks of carbon dioxide detected by FT-IR after their cleavage. In contrast, compounds such as CCBOE9, CCBOE11, and CCBOE12, which are not associated with the generation of carbon dioxide, showed less satisfactory results in their radical photopolymerization compared to the aforementioned three highly active radicals. This is directly related to the higher ability of acyloxy groups to decarboxylate compared to the aryloxy ones. While the absorption peaks of carbon dioxide produced after the cleavage of the remaining compounds can be detected, they are not as prominent as those of CCBOE1, CCBOE4, and CCBOE5. Moreover,

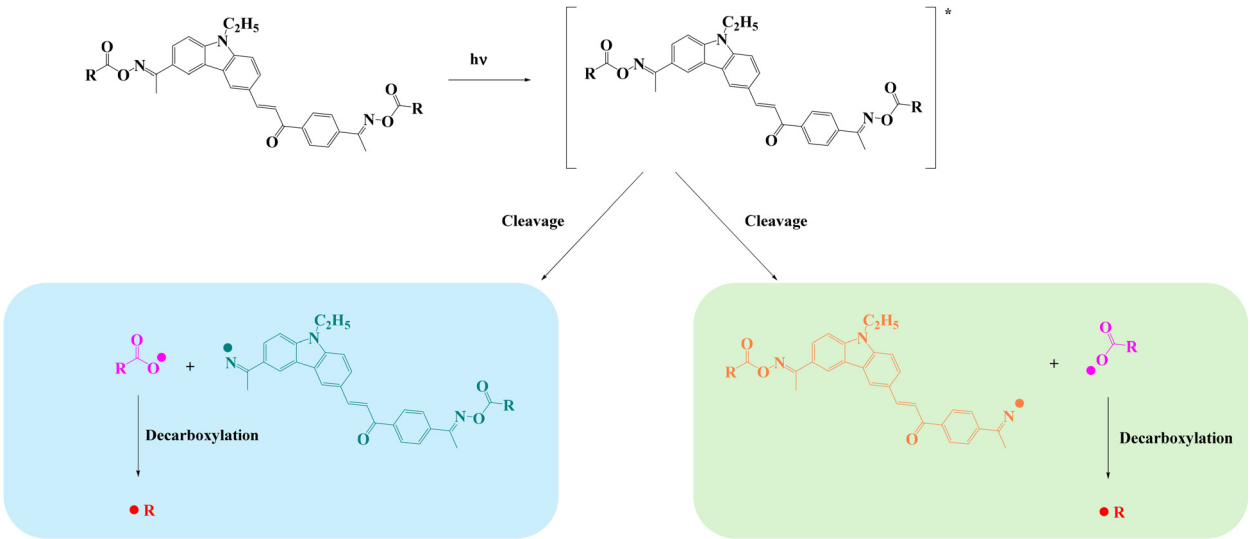

Scheme 2 Suggested mechanism of free radical generation under visible light radiation.

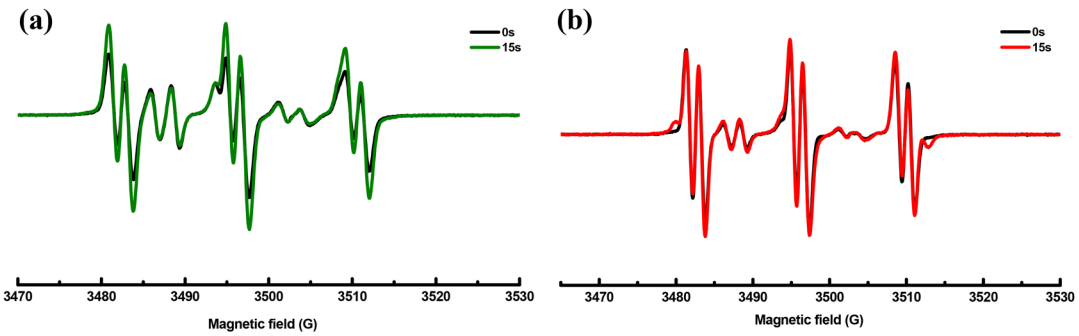

Fig. 4 ESR-ST spectra of the PBN radical adducts of CCBOE4 (a) and CCBOE5 (b) under LED@405 nm irradiation in *tert*-butylbenzene.

the activity of the radicals generated after decarboxylation of these compounds is not as high as that of the aforementioned three OXEs, resulting in relatively low final monomer conversions in triggering TMPTA polymerization.

B.7 Thermal initiation ability

OXEs can not only undergo a photocleavage of the N–O bond upon light excitation, but these structures can also be thermally cleaved by using the appropriate temperature.[47] The conditions used for investigating the thermal initiation abilities of the different OXEs are detailed in the ESI.† Fig. 5 illustrates the DSC thermograms of CCBOE0, CCBOE1, CCBOE3, CCBOE4, and CCBOE5 (2×10^{-5} mol g^{-1}) in TMPTA. Table S2† presents their initial initiation temperatures ($T_{initial}$), maximum weight loss temperatures (T_{max}), and FCs. The $T_{initial}$ of the CCBOE0/TMPTA system is 101 °C, while the $T_{initial}$ of the other selected CCBOE/TMPTA systems containing oxime ester groups are all below 100 °C. Among them, the CCBOE5/TMPTA system has the highest $T_{initial}$, at 83 °C, while the CCBOE1/TMPTA system has the lowest $T_{initial}$, at only 60 °C. In comparison to the $T_{initial}$, the T_{max} values of

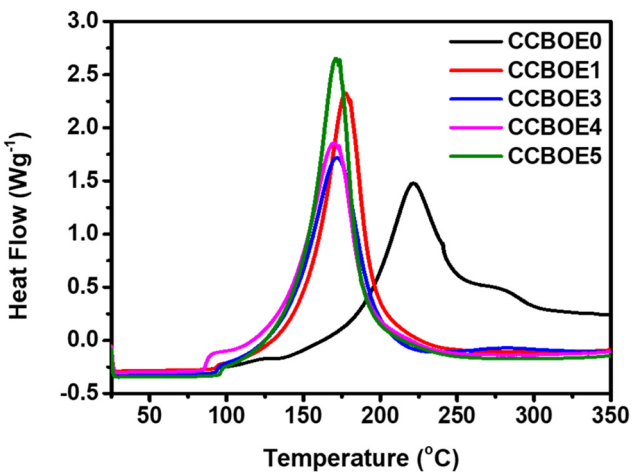

Fig. 5 DSC curves of CCBOE0/TMPTA, CCBOE1/TMPTA, CCBOE3/TMPTA, CCBOE4/TMPTA and CCBOE5/TMPTA systems.

CCBOE1–CCBOE5/TMPTA are similar, ranging between 171 and 179 °C. Compared to the T_{max} of the CCBOE0/TMPTA system (222 °C), the T_{max} of the CCBOE1–CCBOE5/TMPTA

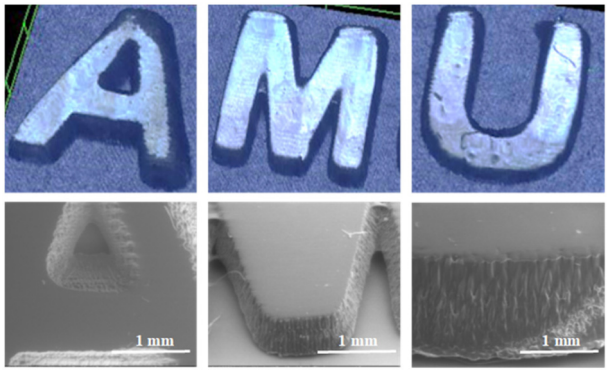

Fig. 6 Characterization of DLW patterns by numerical optical microscopy and SEM.

systems shows a positive trend. This is further supported by the FCs, wherein the polymerization rates of the CCBOE1–CCBOE5/TMPTA systems are all higher than that of the CCBOE0/TMPTA system. Particularly noteworthy is that the CCBOE5/TMPTA system exhibits the highest polymerization rate, reaching 81%. Compared to oxime esters previously reported in the literature and whose structures are summarized in Table S3,† the CCBOEs exhibited lower initial initiation temperatures and higher thermal initiation efficiencies during the free radical polymerization of TMPTA. In the case of CCBOE1 and CCBOE4, their low initiation temperatures of 60 and 65 °C can even constitute a drawback for the long-term storage of these resins, reducing the scope of applications of these two initiators. Overall, CCBOEs are not only suitable for visible light-induced polymerization but also capable of initiating the polymerization of acrylate monomers at temperatures below 100 °C.

B.8 Direct laser writing (DLW)

To assess the CCBOE/TMPTA systems in practical photopolymerization, CCBOE5/TMPTA was deliberately selected, considering its exceptional performance under a 405 nm LED. Using DLW, we created the "AMU" pattern on a small glass plate, and the entire 3D printing process was carried out in an ambient air environment. As shown in Fig. 6, the "AMU" pattern with a thickness of 1000 μm was successfully produced within a brief 2 min period. Through a digital optical microscope and SEM, the contour of the pattern can be clearly observed, indicating the model's extremely high clarity. This is attributed to the rapid cleavage of CCBOE5 under a 405 nm light source, generating two molar equivalents of *tert*-butyl radicals and thereby initiating the highly active polymerization of acrylic ester monomers.

C Conclusions

In summary, a series of innovatively designed and successfully synthesized carbazole–chalcone bis-oxime ester derivatives that have never been reported in the literature before were presented. These CCBOEs exhibited outstanding light absorption performances in the visible range. CCBOE1, CCBOE3, CCBOE4, and CCBOE5 were selected for their superior photopolymerization kinetics, with final conversions reaching 72%, 73%, 72%, and 77%, respectively, after 300 s of 405 nm LED irradiation. These compounds were also tested for their promotion of TMPTA polymerization under 450 nm LED irradiation. Excitingly, after 300 s of 450 nm and 470 nm LED irradiation, the final conversions of CCBOE1 and CCBOE5 all reached 63%, respectively. Based on the experimental results of photopolymerization, the Type I photoinitiator initiation mechanism was proposed, involving photolysis, theoretical calculations, and CO_2 detection. Additionally, CCBOE1, CCBOE3, CCBOE4, and CCBOE5 were also found to be effective in initiating the polymerization of acrylic monomers under thermal conditions. Due to its exceptional performance in the photoinitiation process, CCBOE5/TMPTA, as a representative CCBOE, was successfully utilized for the direct laser writing (DLW) of the "AMU" pattern. The current research unequivocally indicates that increasing the number of oxime ester groups is advantageous for enhancing the photoinitiating efficiency of chalcone-based OXEs during the visible light-induced polymerization of acrylate monomers. Furthermore, they exhibit exceptional photoinitiating kinetics under blue light excitation. Future advancements will necessitate the design of novel chalcone-based bisOXEs, diversifying the structure by modifying the chromophore structures, such as with triphenylamine and phenothiazine. Additionally, the investigation of oxime ester group cleavage activity when excited at longer wavelengths will be pursued.

Conflicts of interest

The authors declare no competing financial interest

Acknowledgements

This research project was supported by the ANR PhotoFlat and the China Scholarship Council (CSC No. 202108330076).

References

1 M. Kaur and A. Srivastava, Photopolymerization: A review, *J. Macromol. Sci., Part C: Polym. Rev.*, 2002, **42**(4), 481–512.
2 G. Oster and N.-L. Yang, Photopolymerization of vinyl monomers, *Chem. Rev.*, 1968, **68**(2), 125–151.
3 J. Shao, Y. Huang and Q. Fan, Visible light initiating systems for photopolymerization: status, development and challenges, *Polym. Chem.*, 2014, **5**(14), 4195–4210.
4 A. Ribas-Massonis, M. Cicujano, J. Duran, E. Besalu and A. Poater, Free-radical photopolymerization for curing products for refinish coatings market, *Polymers*, 2022, **14**(14), 2856.

5 E. Andrzejewska, Free radical photopolymerization of multifunctional monomers, in *Three-Dimensional Microfabrication Using Two-Photon Polymerization*, 2016, Elsevier, pp. 62–81.
6 T. M. Lovestead, A. K. O'Brien and C. N. Bowman, Models of multivinyl free radical photopolymerization kinetics, *J. Photochem. Photobiol., A*, 2003, **159**(2), 135–143.
7 O. Llorente, A. Agirre, I. Calvo, M. Olaso, R. Tomovska and H. Sardon, Exploring the advantages of oxygen-tolerant thiol-ene polymerization over conventional acrylate free radical photopolymerization processes for pressure-sensitive adhesives, *Polym. J.*, 2021, **53**(11), 1195–1204.
8 M. Lang, S. Hirner, F. Wiesbrock and P. Fuchs, A review on modeling cure kinetics and mechanisms of photopolymerization, *Polymers*, 2022, **14**(10), 2074.
9 B. L. S. Vicentin and E. Di Mauro, Free radicals and polymerization of resinous materials used in dentistry, *Electron Spin Resonance Spectroscopy in Medicine*, 2019, pp. 103–133.
10 X. Xu, A. Awad, P. Robles-Martinez, S. Gaisford, A. Goyanes and A. W. Basit, Vat photopolymerization 3D printing for advanced drug delivery and medical device applications, *J. Controlled Release*, 2021, **329**, 743–757.
11 Y. Bao, Recent trends in advanced photoinitiators for vat photopolymerization 3D printing, *Macromol. Rapid Commun.*, 2022, **43**(14), 2200202.
12 S. M. Müller, S. Schlögl, T. Wiesner and M. Haas, Recent advances in Type I photoinitiators for visible light induced photopolymerization, *ChemPhotoChem*, 2022, **6**(11), e202200091.
13 F. Dumur, Recent Advances on Glyoxylates and Related Structures as Photoinitiators of Polymerization, *Macromol. Rapid Commun.*, 2023, **3**(2), 149–174.
14 X. He, Y. Gao, J. Nie and F. Sun, Methyl Benzoylformate Derivative Norrish Type I Photoinitiators for Deep-Layer Photocuring under Near-UV or Visible LED, *Macromolecules*, 2021, **54**(8), 3854–3864.
15 F. Hammoud, A. Hijazi, M. Schmitt, F. Dumur and J. Lalevée, A review on recently proposed oxime ester photoinitiators, *Eur. Polym. J.*, 2023, **188**, 111901.
16 Z. Liu and F. Dumur, Recent advances on visible light Coumarin-based oxime esters as initiators of polymerization, *Eur. Polym. J.*, 2022, **177**, 111449.
17 F. Dumur, Recent advances on carbazole-based oxime esters as photoinitiators of polymerization, *Eur. Polym. J.*, 2022, **175**, 111330.
18 M. Ibrahim-Ouali and F. Dumur, Recent advances on chalcone-based photoinitiators of polymerization, *Eur. Polym. J.*, 2021, **158**, 110688.
19 N. Giacoletto and F. Dumur, Recent advances in bis-chalcone-based photoinitiators of polymerization: from mechanistic investigations to applications, *Molecules*, 2021, **26**(11), 3192.
20 H. Chen, G. Noirbent, S. Liu, D. Brunel, B. Graff, D. Gigmes, Y. Zhang, K. Sun, F. Morlet-Savary, P. Xiao, F. Dumur and J. Lalevée, Bis-chalcone derivatives derived from natural products as near-UV/visible light sensitive photoinitiators for 3D/4D printing, *Mater. Chem. Front.*, 2021, **5**(2), 901–916.
21 S. Liu, Y. Zhang, K. Sun, B. Graff, P. Xiao, F. Dumur and J. Lalevée, Design of photoinitiating systems based on the chalcone-anthracene scaffold for LED cationic photopolymerization and application in 3D printing, *Eur. Polym. J.*, 2021, **147**, 110300.
22 M.-A. Tehfe, F. Dumur, P. Xiao, M. Delgrove, B. Graff, J.-P. Fouassier, D. Gigmes and J. Lalevée, Chalcone derivatives as highly versatile photoinitiators for radical, cationic, thiol–ene and IPN polymerization reactions upon exposure to visible light, *Polym. Chem.*, 2014, **5**(2), 382–390.
23 S. Ohno, M. Yokota, H. Yamada and F. Tatsuzawa, Identification of chalcones and their contribution to yellow coloration in dahlia (Dahlia variabilis) ray florets, *Hortic. J.*, 2021, **90**(4), 450–459.
24 X. Wang, S. Luo, Q. Li, L. Song, W. Zhang, P. Yu, S. Xuan, Y. Wang, J. Zhao, X. Chen and S. Shen, Delphinidins and Naringenin Chalcone Underlying the Fruit Color Changes during Maturity Stages in Eggplant, *Agronomy*, 2022, **12**(5), 1036.
25 Y. Morita, Y. Morita, K. Takagi, M. Fukuchi-Mizutani, K. Ishiguro, Y. Tanaka, E. Nitasaka, M. Nakayama, N. Saito, T. Kagami, A. Hoshino and S. Iida, A chalcone isomerase–like protein enhances flavonoid production and flower pigmentation, *Plant J.*, 2014, **78**(2), 294–304.
26 B. Salehi, C. Quispe, I. Chamkhi, N. El Omari, A. Balahbib, J. Sharifi-Rad, A. Bouyahya, M. Akram, M. Iqbal, A. Oana Docea, C. Caruntu, G. Leyva-Gómez, A. Dey, M. Martorell, D. Calina, V. López and F. Les, Pharmacological properties of chalcones: a review of preclinical including molecular mechanisms and clinical evidence, *Front. Pharmacol.*, 2021, **11**, 592654.
27 N. A. A. Elkanzi, H. Hrichi, R. A. Alolayan, W. Derafa, F. M. Zahou and R. B. Bakr, Synthesis of chalcones derivatives and their biological activities: a review, *ACS Omega*, 2022, **7**(32), 27769–27786.
28 G. Rajendran, D. Bhanu, B. Aruchamy, P. Ramani, N. Pandurangan, K. Naidu Bobba, E. J. Oh, H. Y. Chung, P. Gangadaran and B.-C. Ahn, Chalcone: A promising bioactive scaffold in medicinal chemistry, *Pharmaceuticals*, 2022, **15**(10), 1250.
29 L. Claisen and A. Claparede, Condensationen von ketonen mit aldehyden, *Ber. Dtsch. Chem. Ges.*, 1881, **14**(2), 2460–2468.
30 J. G. Schmidt, Ueber die Einwirkung von Aceton auf Furfurol und auf Bittermandelöl bei Gegenwart von Alkalilauge, *Ber. Dtsch. Chem. Ges.*, 1881, **14**(1), 1459–1461.
31 D. G. Powers, D. S. Casebier, D. Fokas, W. J. Ryan, J. R. Troth and D. L. Coffen, Automated parallel synthesis of chalcone-based screening libraries, *Tetrahedron*, 1998, **54**(16), 4085–4096.
32 J. Li, H. Lu, H. Zheng, X. Zhou, J. Nie and X. Zhu, Thermally activated pyrrole chalcone free radical photoinitiator with excellent stability to sunlight, *Eur. Polym. J.*, 2022, **162**, 110884.

33 H. Chen, G. Noirbent, K. Sun, D. Brunel, D. Gigmes, F. Morlet-Savary, Y. Zhang, S. Liu, P. Xiao, F. Dumur and J. Lalevée, Photoinitiators derived from natural product scaffolds: monochalcones in three-component photoinitiating systems and their applications in 3D printing, *Polym. Chem.*, 2020, **11**(28), 4647–4659.

34 W. Lu, G. Ma and J. Qu, Novel bis-chalcone-based carbazole derivative photoinitiators for visible light polymerization with good photobleaching and biocompatibility, *Prog. Org. Coat.*, 2024, **187**, 108102.

35 B. Bao, J. You, D. Li, H. Zhan, L. Zhang, M. Li and T. Wang, Double benzylidene ketones as photoinitiators for visible light photopolymerization, *J. Photochem. Photobiol., A*, 2022, **429**, 113938.

36 X. Wu, S. Gong, Z. Chen, J. Hou, Q. Liao, Y. Xiong, Z. Li and H. Tang, Photobleachable bis-chalcones-based oxime ester dyes for radical visible photopolymerization, *Dyes Pigm.*, 2022, **205**, 110556.

37 X. Zhang, Z. Liu, D. Zhu, X. Peng, D. Gigmes, M. Schmitt, P. Xiao, F. Dumur and J. Lalevée, Photoinitiating Ability of Pyrene–Chalcone–Based Oxime Esters with Different Substituents, *Macromol. Chem. Phys.*, 2023, **224**(20), 2300293.

38 Y. Zhang, F. Morlet-Savary, M. Schmitt, B. Graff, A. Rico, M. Ibrahim-Ouali, F. Dumur and J. Lalevée, Photoinitiation behavior of phenothiazines containing two oxime ester functionalities (OXEs) in free radical photopolymerization and 3D printing application, *Dyes Pigm.*, 2023, **215**, 111202.

39 D. Oprych, C. Schmitz, C. Ley, X. Allonas, E. Ermilov, R. Erdmann and B. Strehmel, Photophysics of up–conversion nanoparticles: radical photopolymerization of multifunctional methacrylates comprising blue–and UV–sensitive photoinitiators, *ChemPhotoChem*, 2019, **3**(11), 1119–1126.

40 A.-H. Bonardi, S. Zahouily, C. Dietlin, B. Graff, F. Dumur, M. Ibrahim-Ouali, D. Gigmes and J. Lalevée, Thermal initiators as additives for photopolymerization of methacrylates upon blue light, *Coatings*, 2020, **10**(5), 478.

41 S. Liu, N. Giacoletto, B. Graff, F. Morlet-Savary, M. Nechab, P. Xiao, F. Dumur and J. Lalevée, N-naphthalimide ester derivatives as Type I photoinitiators for LED photopolymerization, *Mater. Today Chem.*, 2022, **26**, 101137.

42 S. N. Sidharth, A. R. Yuvaraj, T. J. Hui, B. K. Sarojini, M. Yusoff Mashitah and G. Hegde, Light induced properties of chalcones correlated with molecular structure and photophysical properties for permanent optical storage device, *Adv. Mater. Res.*, 2014, **1033**, 1149–1153.

43 J. Li, H. Zheng, H. Lu, J. Li, L. Yao, Y. Wang, X. Zhou, J. Nie, X. Zhu and Z. Fu, Study on pyrrole chalcone derivatives used for blue LED free radical photopolymerization: Controllable initiating activity achieved through photoisomerization property, *Eur. Polym. J.*, 2022, **176**, 111393.

44 T. Maldonado, G. Ferraudi, A. Graham Lappin and F. Godoy, Kinetic and Mechanistic Observations on the Photoinduced Isomerization Reaction of Organometallic Chalcones: A Steady State and Flash Photolysis Study, *ChemPhotoChem*, 2018, **2**(2), 95–104.

45 T. Borjigin, J. Feng, N. Giacoletto, M. Schmitt, F. Morlet-Savary, B. Graff, P. Xiao, M. Nechab, D. Gigmes, F. Dumur, J. Lalevée, F. Hammoud, A. Hijazi, M. Schmitt, F. Dumur and J. Lalevée, Naphthoquinone-imidazolyl derivatives-based oxime esters as photoinitiators for blue LED-induced free radical photopolymerization, *Eur. Polym. J.*, 2024, **206**, 112801.

46 Z. Liu and F. Dumur, Recent advances on visible light Coumarin-based oxime esters as initiators of polymerization, *Eur. Polym. J.*, 2022, 111449.

47 S. Liu, B. Graff, P. Xiao, F. Dumur and J. Lalevée, Nitro–Carbazole Based Oxime Esters as Dual Photo/Thermal Initiators for 3D Printing and Composite Preparation, *Macromol. Rapid Commun.*, 2021, **42**(15), 2100207.